

## Supplementary Information

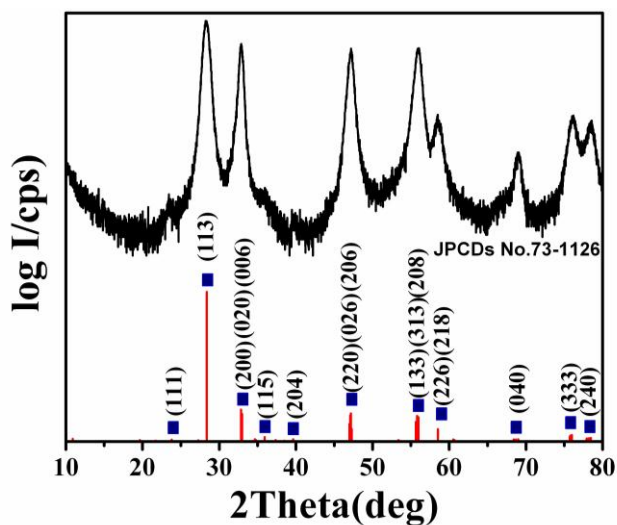


Fig. S1 XRD patterns of as-obtained  $\text{Bi}_2\text{WO}_6$  architectures at 190 °C for 2 h.

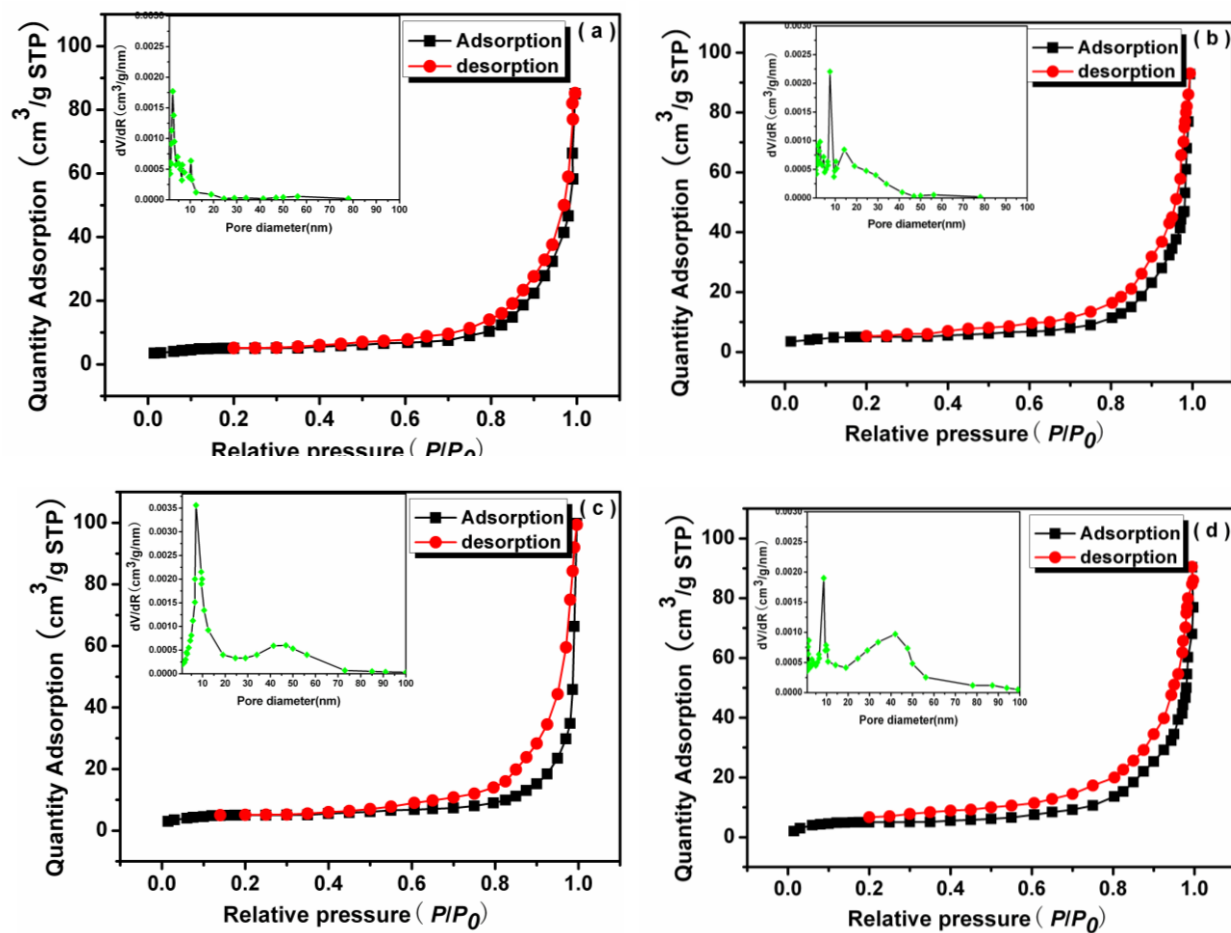
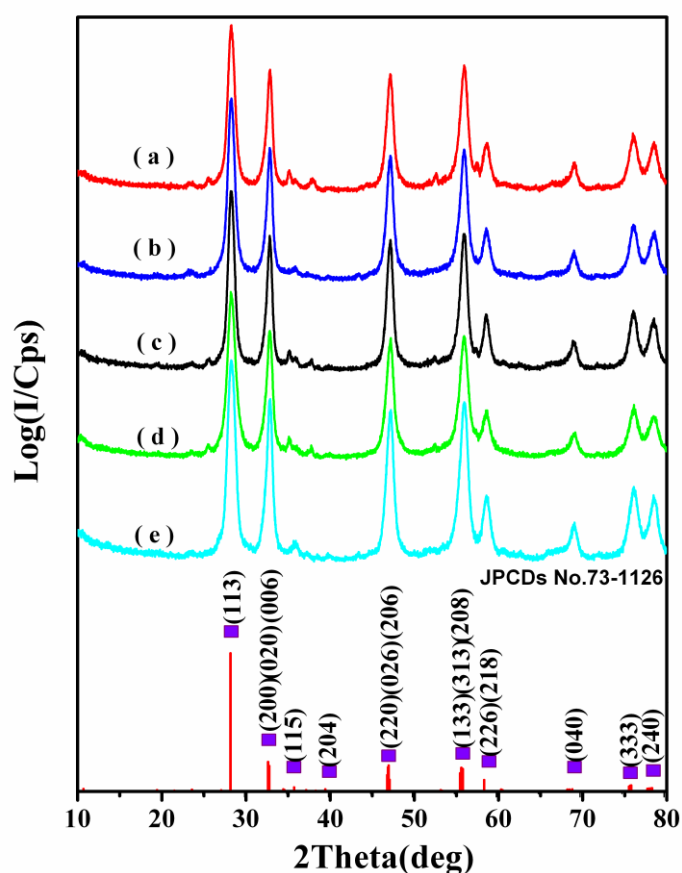


Fig. S2 Nitrogen adsorption-desorption isotherms and the corresponding pore size distribution curve calculated from adsorption branch of the nitrogen isotherm of  $\text{Bi}_2\text{WO}_6$ . (a)S0.5, (b)S1, (c)S2, (d)

S6.

The specific surface areas of as-synthesized samples under different hydrothermal reaction time were given in Fig.S2. The specific surface areas of the samples prepared at 190 °C for 0.5 h and 1.0 h are 25.6 m<sup>2</sup>·g<sup>-1</sup> and 32.6 m<sup>2</sup>·g<sup>-1</sup>, respectively (Figs.S2 a-b). The largest surface area of 47.72 m<sup>2</sup>·g<sup>-1</sup> is achieved when the sample was synthesized at 190 °C for 2.0 h (Fig.S2c). Expanding the hydrothermal treatment time to 6 h, BET surface area of the products have no obvious change, the value is 46.5 m<sup>2</sup>·g<sup>-1</sup>.



**Fig. S3** XRD patterns of as-synthesized Bi<sub>2</sub>WO<sub>6</sub> under different pH values at 190 °C for 2h. (a) pH 1, (b) pH 3, (c) pH 5, (d) pH 7, (e) pH 9.

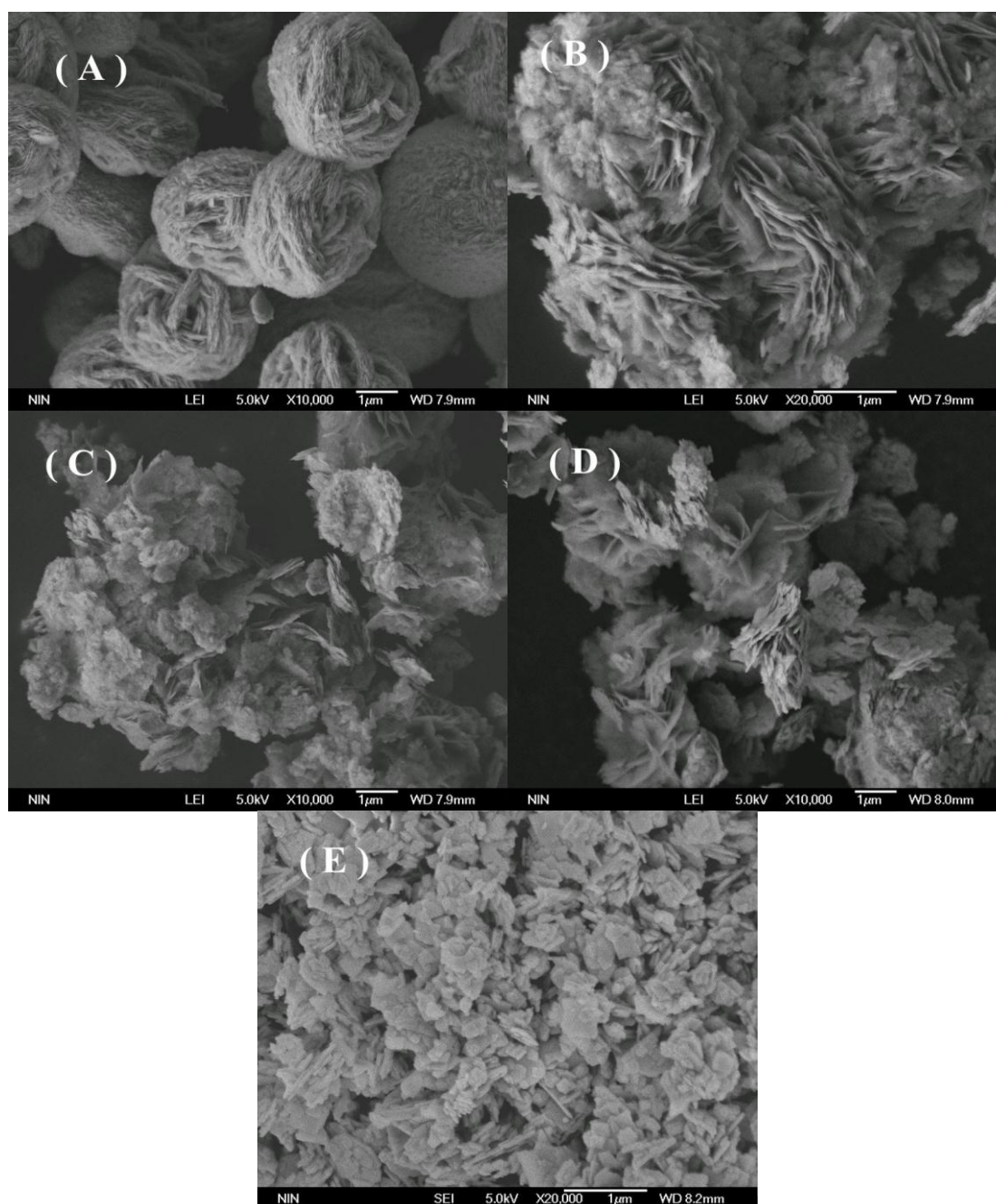
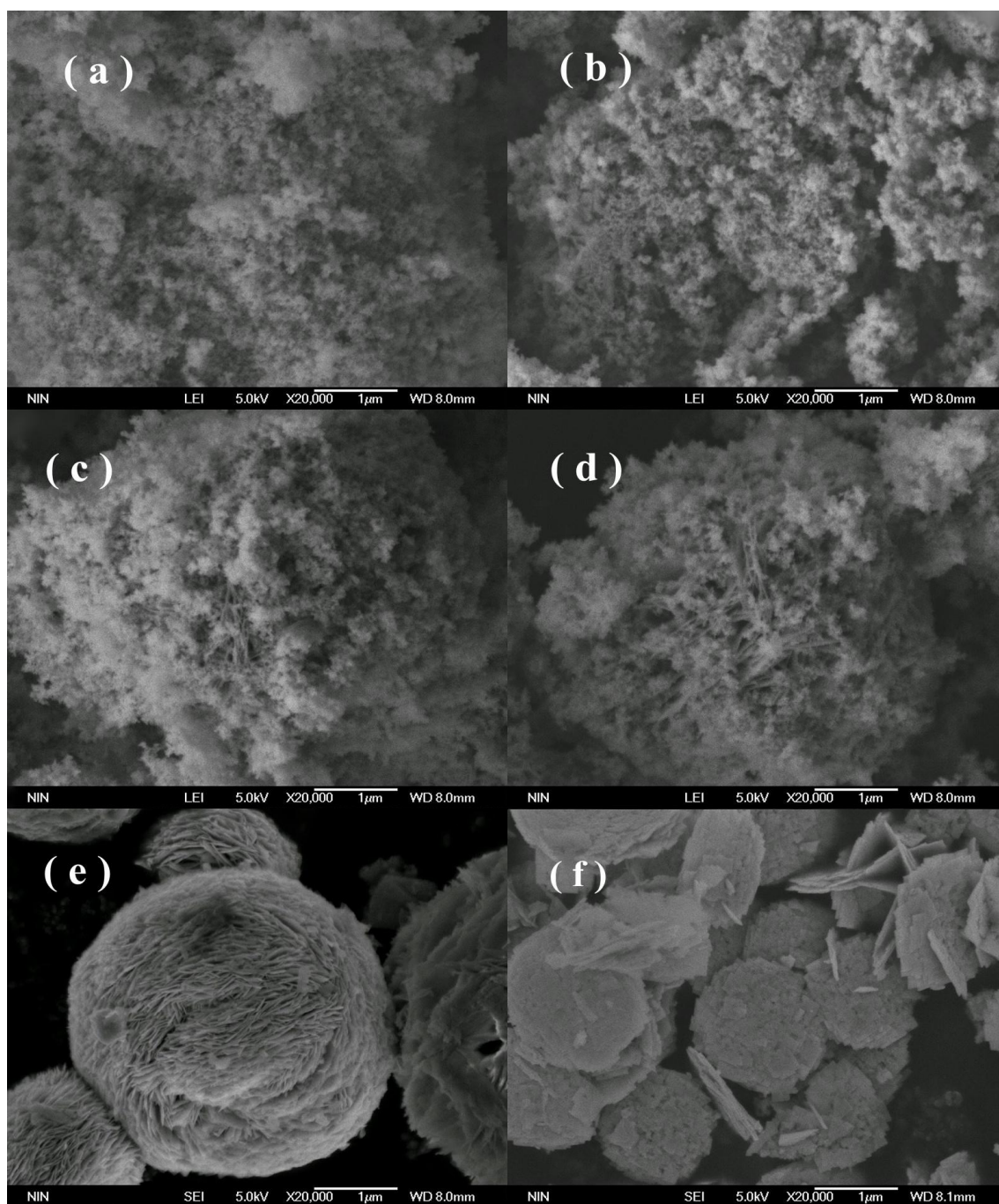


**Fig. S4** FE-SEM picture of as-synthesized  $\text{Bi}_2\text{WO}_6$  under different pH at  $190^\circ\text{C}$  for 2h.

(a) pH 1, (b) pH 3, (c) pH 5, (d) pH 7, (e) pH 9.

**Fig. S3** indicates that all of the samples can be readily indexed to an orthorhombic  $\text{Bi}_2\text{WO}_6$  (JCPD file no.73-1162). No characteristic peaks of other impurities were observed. The products have high crystallinity under different pH value. When the pH value increase from 1.0 to 3.0 while fixing the other hydrothermal conditions constant, the morphology of  $\text{Bi}_2\text{WO}_6$  is shown in **Fig. S4**, from which the flower-like  $\text{Bi}_2\text{WO}_6$  nanostructure can be observed while nest-like nanostructure is disappeared. Increasing the pH value to 5.0 and 7.0, the morphology of the hydrothermal product is

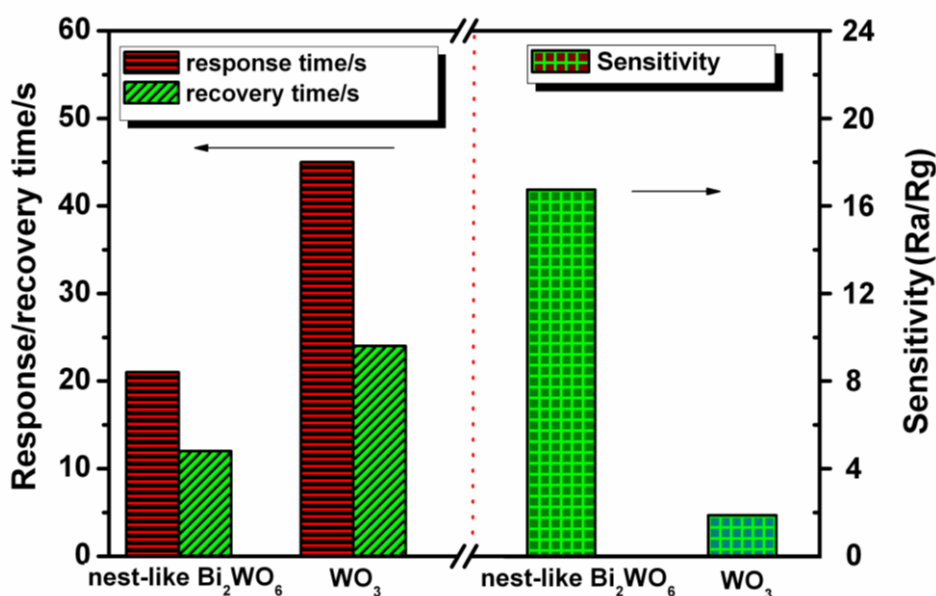
distinctly different. It can be seen that the multidisc-like  $\text{Bi}_2\text{WO}_6$  nanostructure are the mainly products. As the pH value continues to increase to 9.0, the three-dimensional structures are fallen apart. The nanoplates of  $\text{Bi}_2\text{WO}_6$  are randomly piled up with no typical aggregation.



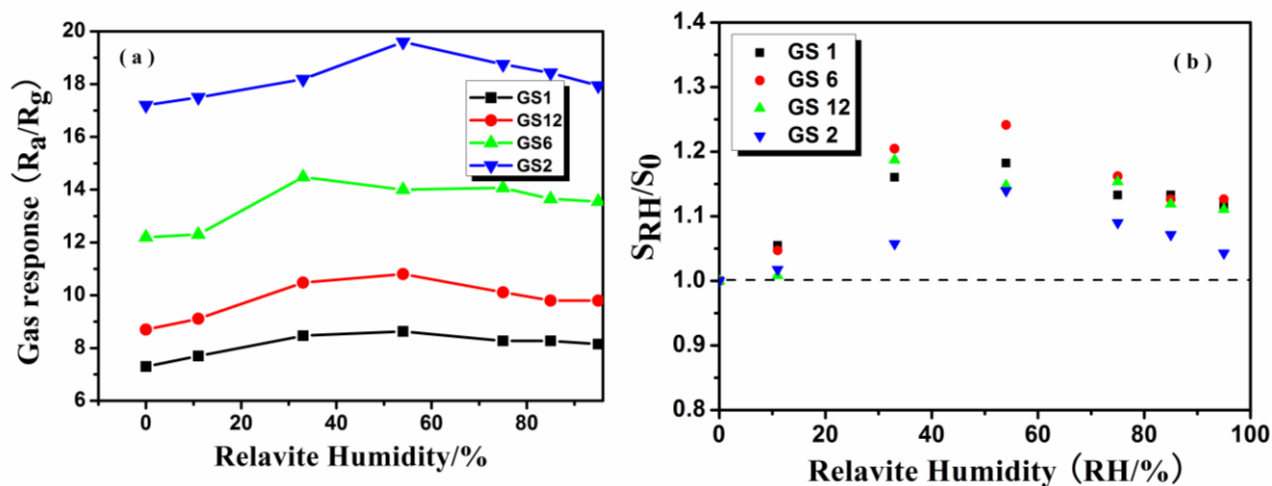
**Fig. S5** FE-SEM images of the samples prepared by hydrothermal process at different temperature for 2h by using  $(\text{NH}_4)_{10}\text{W}_{12}\text{O}_{41}\cdot 5\text{H}_2\text{O}$  and  $\text{Bi}(\text{NO}_3)_3$  as starting materials: ( a ) 140°C, ( b ) 160°C, ( c ) 170°C, and ( d ) 180°C and ( e ) 190°C. And the obtained sample ( f ) prepared by hydrothermal process at 190 °C for 12 h by using  $\text{Na}_2\text{WO}_4\cdot 2\text{H}_2\text{O}$  and  $\text{Bi}(\text{NO}_3)_3$  as starting materials.

Figure S5 shows the FE-SEM images of samples obtained under different hydrothermal

temperature for 2 h. As shown in [Figures S5](#), the samples exhibit sphere-like nanoparticles with the size of about 20 to 50 nm under 140 °C and 160 °C, respectively. Further increased the hydrothermal temperatures to 170 °C and 180 °C, the obtained samples begin to appear the plate-like morphology, which indicates that the  $\text{Bi}_2\text{WO}_6$  nanoparticles begin to grow along the certain direction. Continue to increase the hydrothermal temperature to 180 °C, more and more plate-like morphology  $\text{Bi}_2\text{WO}_6$  was formed coexisting with a mass of spherical nanoparticles. [Figure S5\(e\)](#) shows the FE-SEM images of  $\text{Bi}_2\text{WO}_6$  obtained under 190 °C hydrothermal reactions for 2 h. It can be seen that as-obtained  $\text{Bi}_2\text{WO}_6$  exhibit an uniform nest-like 3D  $\text{Bi}_2\text{WO}_6$  nanostructure with scales of 3~4  $\mu\text{m}$ . The above results indicated that the hydrothermal temperature is vital to the formation of novel nest-like  $\text{Bi}_2\text{WO}_6$  nanostructure. Fixed the other condition unchanged, only using  $\text{Na}_2\text{WO}_4 \cdot 5\text{H}_2\text{O}$  instead of  $(\text{NH}_4)_{10}\text{W}_{12}\text{O}_{41} \cdot 5\text{H}_2\text{O}$ , FE-SEM image of the resulted sample is shown in [Figure S5 \(f\)](#). Interestingly, the as-obtained sample exhibits multilayer-disk morphology after hydrothermal reaction. So, we can draw conclusion that the species of tungsten source is also vital to the formation the 3D nest-like  $\text{Bi}_2\text{WO}_6$  nanostructure.



**Fig. S6** Comparison of responses/recovery time and sensitivity of as-fabricated 3D mesoporous nest-like  $\text{Bi}_2\text{WO}_6$  ( $\text{Bi}_2\text{WO}_6$ -2h) gas sensor and mesoporous  $\text{WO}_3$  based gas sensor when operated at 300 °C. (Concentration of ethanol, 20 ppm, RH 0%).



**Fig. S7** Effect of relative humidity on the response of Bi<sub>2</sub>WO<sub>6</sub> based gas sensors to ethanol when operated at 300 °C. (Concentration of ethanol, 20 ppm,  $S_{RH}$  is the sensitivity value at certain RH value,  $S_0$  is the sensitivity value at RH = 0%).